Bulletin de la Société Royale des Sciences de Liège, Vol. 80, 2011, p. 724 - 728

The variable X-ray spectrum of the Wolf-Rayet binary WR140 with Suzaku

Yasuharu Sugawara[1], Yoshitomo Maeda[2], Yohko Tsuboi[1], Kenji Hamaguchi[3,4], Michael Corcoran[3,5], Andy Pollock[6], Anthony Moffat[7], Peredur Williams[8], Sean Dougherty[9] and Julian Pittard[10]

[1] Department of Physics, Chuo University, Japan
[2] Department of High Energy Astrophysics, ISAS/JAXA
[3] CRESST and X-ray Astrophysics Laboratory NASA/GSFC
[4] Department of Physics, University of Maryland
[5] Universities Space Research Association
[6] European Space Agency, XMM-Newton Science Operations Centre
[7] D*é*partement de Physique, Universit*é* de Montr*é*al
[8] Institute for Astronomy, Royal Observatory Edinburgh
[9] National Research Council of Canada
[10] School of Physics and Astronomy, The University of Leeds

Abstract: We report the preliminary results of the Suzaku observations of the W-R binary WR 140 (WC7+O5I). We executed the observations at four different epochs around periastron passage in Jan. 2009 to understand the W-R stellar wind as well as the wind-wind collision shocks. The total exposure was 210 ks. We detected hard X-ray excess in the HXD band ($>$ 10 keV) for the first time from a W-R binary. Another notable discovery was a soft component which is less absorbed even by the dense wind. The spectra can be fitted by three different components; one is for the cool component with kT=0.1–0.6 keV, one for a dominant high-temperature component with kT $\sim$3 keV, and one for the hardest power-law component with the photon index of $\sim$2. As periastron approached, the column density of the high-temperature component increased, which can be explained as self-absorption by the W-R wind. The emission measure of the dominant, high-temperature component is not inversely proportional to the distance between the two stars.

1 Introduction

The Wolf-Rayet binary WR140 (WC7+O5I) has an extremely eccentric (e =0.88) orbit with long orbital period (P=7.94 yrs; Marchenko et al. 2003). The Suzaku AO-3 cycle covered the periastron passage, when physical parameters change the most dramatically. We executed X-ray monitoring observations around periastron passage to measure the change of the conditions in the hot post-shock gas.

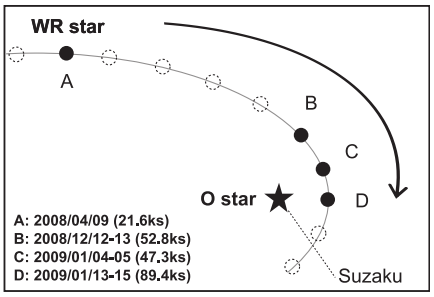

Figure 1: The geometry at the epochs of the four observations.

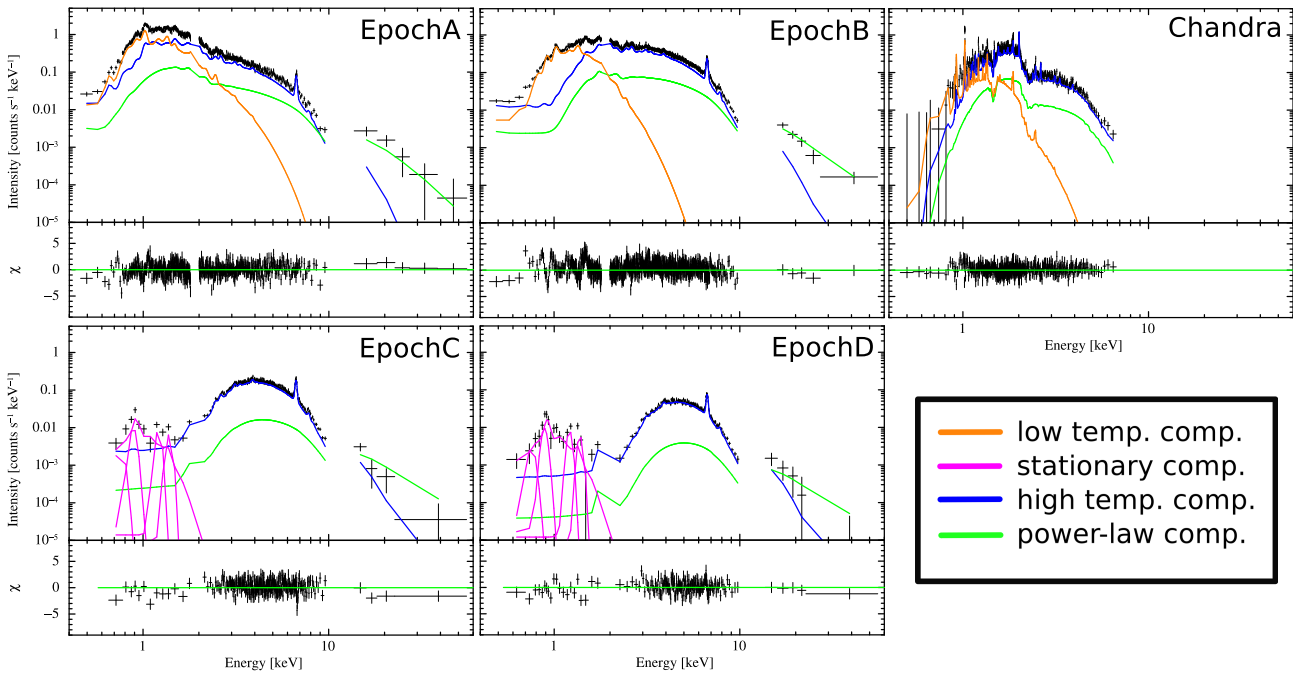

Figure 2: The XIS and HXD-PIN spectra of WR140 at each epoch. Backgrounds are subtracted. The model components are separately indicated in the upper panels. Lower panels show the residuals of the data from the best-fit model(Table 1). We fitted simultaneously the spectra of the epoch A and B, together with those of Chandra.

2 Observations & Analysis

We observed WR140 with Suzaku at four different epochs around periastron passage in Jan. 2009. The total exposure time was 210 ks. Figure 1 shows the observational geometries and the X-ray spectra at the four epochs, respectively. We adopted the orbital solution in Marchenko et al. (2003). The spectra below $E = 10$ keV were obtained with XIS, and those above 10 keV were with HXD-PIN. The flux and spectral shape of the X-ray spectra varied with the epochs. In spite of the variation, lines from highly ionized ions of oxygen, neon, magnesium, silicon, sulphur, argon, calcium, iron and nickel are detected. They are attributed to the emission from the optically thin thermal plasma as seen in the previous satellite observations.

Figure 2 shows that soft X-ray absorption varied with phase and is lowest at epoch A (phase=2.904) and largest at epoch D (phase=3.000). It is naturally explained that the main component of the X-ray emission is deeply embedded in the WR 140 binary system and is self-absorbed by the WR-wind (cf., Zhekov & Skinner 2000). We modeled the WR-wind absorption with a photoelectric absorption code with variable abundances, varabs. XSPEC package version 12.5 is used in the analysis of the spectra. We also added an absorption model, TBabs (Wilms, Allen & McCray 2000) to take into account the

interstellar absorption. The solar abundances by Wilms et al. (2000) were adopted. The interstellar absorption column density was determined from the spectrum at epoch A.

In addition to the Suzaku data, we used archived Chandra data. WR 140 was observed with the Chandra HETGS on 2000 December 29 beginning at 10:13:28 (ObsID 2337), with a total integration time 45.5 ks. Pollock et al. (2005) reported the results of this spectral analysis. The HETG spectra are very sensitive to the line emission and works to constrain the abundance of the plasma. Since this Chandra observation (phase=1.987) was made at the similar epoch of the Suzaku epoch B (phase=2.989), the spectra of the Suzaku epoch A, B and the 2000 Chandra were simultaneously fit to the same models with the some parameters allowed to vary (Table 1). But, this method may require validation to consider the variable nature of X-ray emission.

Table 1: Results of spectral fitting with the three components of models. Errors and upper limits are at 90% confidence level.

Epoch	A	B	Chandra	C	D
Orbital phase	2.904	2.989	1.987	2.997	3.000
interstellar absorption (TBabs)					
$N_{\rm H}$ (10^{21} cm^{-2})		$8.59^{+0.02}_{-0.01}$		8.59(fixed)	
low-temperature component (varabs*vpshock)					
$N_{\rm He}^{\rm LT}$ (10^{19} cm^{-2})	–	2.5±0.1	2.2±0.4	–	–
$k_{\rm B}T_{\rm LT}$ (keV)	$0.656^{+0.007}_{-0.010}$	$0.3511^{+0.0002}_{-0.0006}$		–	–
τ_u($\times 10^{12}$ s cm^{-3})	$4.1^{+0.4}_{-0.3}$	$3.9^{+0.6}_{-0.3}$		–	–
norm [1]($\times 10^{-3}$)	$7.4^{+0.1}_{-0.4}$	$14.5^{+0.2}_{-0.7}$	10^{+2}_{-1}	–	–
$L_{\rm X}$ [2]($\times$ 10^{34} erg s^{-1})	2.32	6.11	4.33	–	–
high-temperature component (varabs*vpshock)					
$N_{\rm He}^{\rm HT}$ (10^{20} cm^{-2})	≤ 0.006	$1.74^{+0.03}_{-0.01}$	5.3±0.4	$12.6^{+0.2}_{-0.1}$	$23.1^{+0.6}_{-0.2}$
$k_{\rm B}T_{\rm HT}$ (keV)	$2.73^{+0.03}_{-0.06}$	$3.03^{+0.02}_{-0.03}$		$2.60^{+0.08}_{-0.06}$	$2.73^{+0.07}_{-0.13}$
τ_u($\times$ 10^{12} s cm^{-3})	4.1^{4}	3.9^{4}		$1.8^{+1.0}_{-0.5}$	$1.7^{+1.4}_{-0.8}$
norm [1]($\times 10^{-2}$)	$1.09^{+0.04}_{-0.01}$	$2.97^{+0.03}_{-0.05}$	$3.54^{+0.05}_{-0.06}$	$3.57^{+0.11}_{-0.07}$	$1.89^{+0.10}_{-0.09}$
$L_{\rm X}$ [2]($\times$ 10^{34} erg s^{-1})	2.01	5.57	6.68	8.23	4.44
power-law component					
Γ		$1.93^{+0.02}_{-0.03}$		1.93(fixed)	
norm [5] ($\times$ 10^{-3})	$1.98^{+0.06}_{-0.02}$	$4.69^{+0.01}_{-0.04}$		2.3±0.4	$1.0^{+0.3}_{-0.5}$
$L_{\rm X}$ [2]($\times$ 10^{33} erg s^{-1})	0.71	1.67		0.79	0.34
stationary component (varabs*(apec+5redge))					
$N_{\rm He}^{\rm S}$ (10^{19} cm^{-2})	–	–	–	1.4(fixed)	
$k_{\rm B}T_{\rm S}$ (keV)	–	–	–	0.13(fixed)	
norm [1]($\times 10^{-3}$)	–	–	–	14(fixed)	
$k_{\rm B}T_{\rm RRC}$ (eV)	–	–	–	12(fixed)	
norm$_{\rm C\ VI}$ [3]($\times 10^{-2}$)	–	–	–	1.6(fixed)	
norm$_{\rm O\ VII}$ [3]($\times 10^{-4}$)	–	–	–	3.1(fixed)	
norm$_{\rm O\ VIII}$ [3]($\times 10^{-4}$)	–	–	–	1.5(fixed)	
norm$_{\rm Ne\ IX}$ [3]($\times 10^{-5}$)	–	–	–	1.5(fixed)	
norm$_{\rm Ne\ X}$ [3]($\times 10^{-6}$)	–	–	–	7.4(fixed)	
$L_{\rm X}$ [2]($\times$ 10^{35} erg s^{-1})	–	–	–	1.1	
χ^2/dof		4424.50/3230		619.95/499	338.48/292

[1] Normalization constant defined as $\mathrm{EM} \times 10^{-14}(4\pi \mathrm{D}^2)^{-1}$, where EM is the emission measure in cm^{-3} and D is the distance in cm.

[2] The absorption-corrected luminosity (0.5–50.0 keV) was calculated assuming a distance of 1.85 kpc.

[3] Normalization constant of the redge model defined as total photons cm^{-2} s^{-1} in the line.

[4] Ionization timescale of high temperature component is linked to that of low temperature component.

[5] Normalization constant of the power-law model defined as photons keV^{-1} cm^{-2} s^{-1} at 1 keV.

2.1 Spectral fit at epoch A, B and the 2000 Chandra observation

The single-temperature plane-parallel shock model (vpshock) shows a good fit in the energy band higher than 4 keV. However, the model can not reproduce the line and edge structures which appeared in the soft energy band below ∼3 keV. So we adopted a two-temperature plane-parallel shock model suffering two different absorption column densities. We found that the fitting is significantly improved in the XIS spectra.

At epochs A and B, there further exist residuals in the HXD/PIN data above 10 keV. We then introduce the power-law model as an additional component. The power-law component is only significant in the epoch A spectra. The best-fit power-law index at the epochs A and B is $\Gamma \sim 1.9$. We assumed the same value for the other epochs of C (phase=2.997) and D. The emission may originate from inverse Compton interactions between relativistic electron and stellar UV photons or from thermal bremsstrahlung of higher temperature shock plasma.

No emission lines from helium and carbon ions were identified in the data. For the vpshock models, we assumed the abundance ratio C/He = 0.4 by number, which was taken from Hillier & Miller (1999). Other abundance value except helium, carbon, neon, magnesium and iron were fixed the best-fit values of Pollock et al. (2005). The abundance for the absorption model of $N_{\rm He}$ is linked to that of the vpshock model.

2.2 Spectral fit at epoch C and D

The single-temperature vpshock model shows a good fit in the energy band higher than 2 keV. However, the model can not reproduce the soft excess seen below 2 keV. We then add another soft component of an absorbed single-temperature model. Since the statistics are limited, we assume a plasma in the collisional ionized equilibrium (APEC). Since no significant change in X-ray flux below 1.6 keV were detected, we further assumed the same parameters for this stationary component at both epochs C and D.

The soft component can be fitted with a single-temperature model of $k_{\rm B}T_{\rm S} \sim 0.15$ keV with an absorption column of $N_{\rm He}^{\rm S} \sim 1\times 10^{20}$ cm^{-2}, but some line-like residuals still remained (χ^2/dof of 198/56). We found that the residuals are consistent with those of the recombination edges. So, we introduce the five RRC (redge) models at the energy of C VI(0.499 keV), O VII(0.739 keV), O VIII(0.871 keV), Ne IX(1.196 keV), and Ne X(1.362 keV). The fit was improved to an acceptable χ^2/dof of 68/50. After checking the significance of an F-test for an additional recombination edge model, the RRC structure of Ne IX is the most significant. At the epochs A and B, emissions of a soft component are virtually undetectable due to dominant emissions of other high-temperature component. Therefore, we didn't add a soft component to these best-fit models at epoch A, B and the 2000 Chandra observation.

3 The variation of emission measure

From epoch A to C, the emission measure increased along with the inversely proportional correlation with the separation, d, of two stars. This is consistent with the prediction in the simple colliding wind theory (Usov 1992), which is usually used. On the other hand, from epoch C to D, toward periastron, the emission measure decreased against the prediction. This would mean that we need to introduce one more parameter R, wind momentum flux ratio, $R = \left((\dot{M}v)_{\rm WR}/(\dot{M}v)_{\rm O}\right)^{1/2}$. According to Stevens, Blondin & Pollock (1992), EM can be written as ${\rm EM} \propto d^{-1}\,(1+R)/R^4$.

At periastron, the momentum flux of the O-type star becomes smaller, since the O-star wind cannot reach terminal velocity because of the small distance from the O-star to the shock region, while that

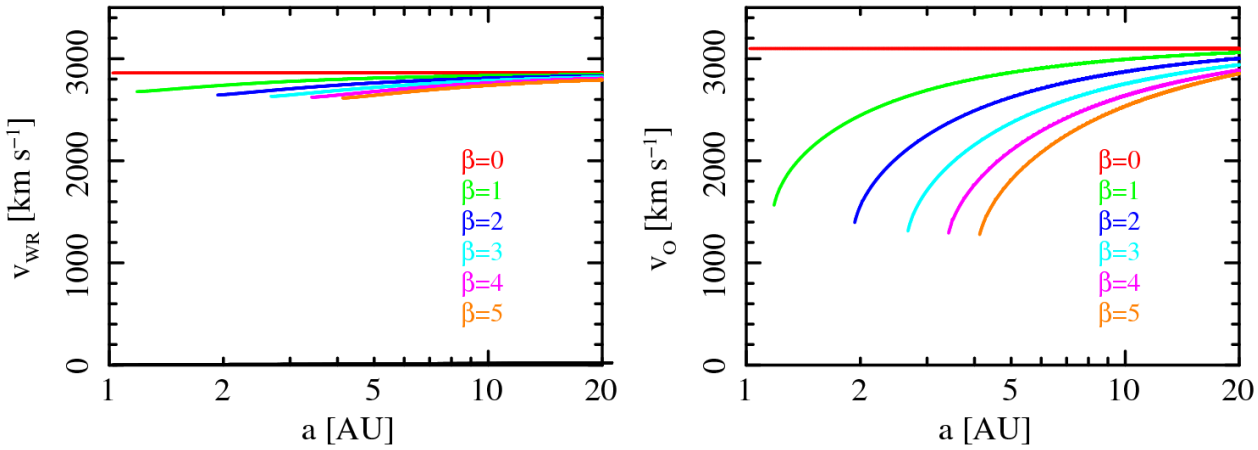

Figure 3: The wind velocity vs. distance (left;W-R star, right;O star).

of the W-R star changes less. In Figure 4, we show the pre-shock stellar wind velocities of the W-R and O stars at a given binary separation. We adopted a simple beta law for the wind acceleration: $v(r) = v_\infty(1 - R_*/r)^\beta$. Here, r, v_∞, and R_* are the distance from stellar surface to shock region, terminal velocity, and stellar radius, respectively. We used the value of $R_*^{\rm WR} = 13\ R_\odot$ (Williams et al. 1990), $R_*^{\rm O} = 26\ R_\odot$ (cf., Williams et al. 2009), $\dot{M}({\rm WR}) = 4.3\times10^{-5}{\rm M}_\odot{\rm yr}^{-1}$ and $\dot{M}({\rm O}) = 8.7\times10^{-6}{\rm M}_\odot{\rm yr}^{-1}$ (Dougherty et al. 2005). The W-R wind reaches near the terminal velocity in any assumption for β while the O-star is far below its terminal value for a large value of β.

In Figure 4, we plot the normalized X-ray emission measure calculated using the equation (EM $\propto d^{-1}\ (1 + R)/R^4$). The emission measure is normalized at the separation of epoch A (15 AU). The wind momentum flux ratio rapidly becomes large near the periastron for the large β. The calculation is truncated near the periastron since the stagnation point reaches the surface of the O star. The sudden drop of the emission measure near epoch D is visible for the case of a slow wind acceleration of $\beta \approx 2$–3.

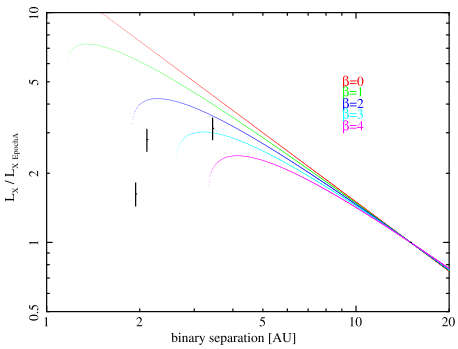

Figure 4: The binary separation vs. normalized X-ray luminosity. Black shows emission measure of a dominant high-temperature component with kT ∼3 keV.

References

Dougherty, S.M., Beasley, A.J., Claussen, M.J., Zauderer, B.A., & Bolingbroke, N.J. 2005, ApJ 623, 447
Hillier, D.J., & Miller, D.L. 1999, ApJ 519, 354
Marchenko, S.V., Moffat, A.F.J., Ballereau, D., et al. 2003, ApJ 596, 1295
Pollock, A.M.T., Corcoran, M.F., Stevens, I.R., & Williams, P.M. 2005, ApJ 629, 482
Stevens, I.R., Blondin, J.M. & Pollock, A.M.T. 1992, ApJ 386, 265
Usov, V.V. 1992, ApJ 389, 635
Wilms, J., Allen, A., & McCray, R. 2000, ApJ 542, 914
Williams, P.M., van der Hucht, K.A., Pollock, A.M.T., Florkowski, D.R., van der Woerd, H., & Wamsteker, W.M. 1990, MNRAS 243, 662
Williams, P.M., Marchenko, S.V., Marston, A.P., et al. 2009, MNRAS 395, 1749
Zhekov, S.A., & Skinner, S.L. 2000, ApJ 538, 808